

SOURCE SCALING FOR INTERMEDIATE-DEPTH VRANCEA EARTHQUAKES WITH EMPIRICAL GREEN'S FUNCTIONS

Adrien Oth¹, Friedemann Wenzel¹ and Mircea Radulian²

ABSTRACT

Several source parameters (source dimensions, slip, particle velocity, static and dynamic stress drop) are determined for the two moderate-size October 27th, 2004 ($M_W=5.8$) and May 14th, 2005 ($M_W=5.2$), and the two large August 30th, 1986 ($M_W=7.1$) and March 4th, 1977 ($M_W=7.4$) Vrancea intermediate-depth earthquakes. For this purpose, the empirical Green's functions method of Irikura (1983, 1986, 1999) is used to generate synthetic time series from recordings of smaller events (with $4 \leq M_W \leq 5$) in order to estimate several parameters characterizing the so-called strong motion generation area (Miyake et al., 2003). The parameters are obtained by acceleration envelope and displacement waveform inversion for the 2004, 2005 and 1986 events and MSK intensity pattern inversion for the 1977 event using a genetic algorithm. The strong motion recordings of the analyzed Vrancea earthquakes as well as the MSK intensity pattern of the 1977 earthquake can be well reproduced using relatively small strong motion generation areas, which corresponds to small asperities with high stress drops (300 – 1200 bar) and high particle velocities (3 – 5 m/s). These results imply a very efficient high-frequency radiation, which has to be taken into account for strong ground motion prediction, and indicate that the intermediate-depth Vrancea earthquakes are inherently different from crustal events.

INTRODUCTION

The Vrancea district, located in the South-Eastern part of the Carpathian arc, is affected by the occurrence of frequent and strong intermediate-depth earthquakes. The peculiarity regarding these earthquakes is the fact that they are all generated within a narrowly confined focal volume, whose epicentral area is limited to an extent of approximately $30 \times 70 \text{ km}^2$. The depth range is limited to a vertical stripe ranging from around 80 to 200 km. The observed focal mechanisms of Vrancea earthquakes (e.g. Oncescu and Bonjer, 1997) as well as the results of a stress inversion by Plenefisch (1996) indicate a thrust regime with vertical extension and horizontal compression. Two types of fault mechanisms are observed. The prevalent type is characterized by a NE-SW striking fault plane and perpendicular maximum compression. All Vrancea events with $M_W \geq 7$ which occurred during the last century show this kind of mechanism. Fewer events have a NW-SE striking fault plane with maximum compression in the NE-SW direction.

The strong seismicity at intermediate-depth beneath Vrancea is associated with a subducted and partially detached slab. The Vrancea earthquakes are interpreted as events within a not yet completely detached slab segment, in a vertical position (e.g. Sperner et al., 2001). This interpretation is compatible with the observed thrust fault mechanisms and is strongly supported by a recent regional tomography study by Martin et al. (2006), which images the slab and shows clear indications that the seismicity is confined to the slab. Wenzel et al. (1999) show that the seismic energy release rate of the Vrancea seismogenic zone is the fourth highest in Europe. Four major shocks with moment magnitudes larger than 6.5 occurred during the last century, namely on November 10, 1940 ($M_W = 7.7$), March 4, 1977 ($M_W = 7.4$), August 30, 1986 ($M_W = 7.1$) and May 30, 1990 ($M_W = 6.9$).

¹ Geophysical Institute, University of Karlsruhe, Germany

² National Institute for Earth Physics, Bucharest, Romania

Especially the former two led to disastrous consequences on Romanian territory. Bucharest was affected by seismic intensities of VIII and VII during the 1977 and 1986 earthquakes, respectively.

We use the empirical Green's functions (EGF) method of Irikura (1983, 1986, 1999) to get more insight into the source parameters (source dimensions, slip, slip velocity, static and dynamic stress drop) of the two moderate earthquakes of October 27th 2004 and May 14th 2005 as well as the large shocks which occurred on August 30th 1986 and March 4th 1977. Whereas the strong motion database for the latter two events is rather sparse (especially for the 1977 event, where only one single observation in Bucharest exists), especially the case study of the October 2004 event is very promising, as the number of high-quality strong motion recordings for this earthquake is by far the largest as ever recorded in Romania.

Among the above-mentioned source parameters, stress drop is of high interest in view of seismic hazard assessment, as it is a key parameter in the estimation of strong ground motion. Following Brune (1970), the dynamic stress drop controls the high frequency level (i.e. beyond the corner frequency) of ground acceleration. This is especially important for earthquake engineering applications, as for large earthquakes, almost the entire frequency band of interest to this discipline lies beyond the corner frequency. The dynamic stress drop $\Delta\sigma_d$ can be linked to the average particle velocity on the fault $\langle\dot{U}\rangle$ by (Kanamori, 1994):

$$\Delta\sigma_d = C_d \frac{\mu}{v_s} \langle\dot{U}\rangle, \quad (1)$$

where C_d is a non-dimensional constant of the order of 2, μ is the shear modulus and v_s the shear wave velocity. The static stress drop, on the other hand, can be related to the strain change \bar{D}/\tilde{L} (with \bar{D} being the average displacement on the fault and \tilde{L} the characteristic source dimension):

$$\Delta\sigma_s = C_s \mu \frac{\bar{D}}{\tilde{L}}, \quad (2)$$

where C_s is a non-dimensional constant whose value depends on the source geometry and the choice of \tilde{L} (Kanamori and Anderson, 1975).

In this study, synthetic time series (acceleration, velocity and displacement) are computed for the moderate to large Vrancea earthquakes mentioned above in a broadband frequency range (about 0.4 – 12 Hz) from smaller events using the EGF-method of Irikura and compared with observed records. As there is only one observation available for the 1977 event, instrumentally determined intensity is compared with the observed macroseismic intensity (MSK) pattern. Minimizing the cost (misfit) between observations and simulations enables us to find suitable models for the strong motion generation area (SMGA, Miyake et al., 2003). A genetic algorithm is used to find acceptable solutions.

DATABASE

All the records from the small earthquakes used as EGF events as well as from the two considered mainshocks which occurred in 2004 and 2005 (the two moderate ones) were gathered by the accelerometer network installed by the Collaborative Research Center 461 (CRC 461) 'Strong Earthquakes: A Challenge for Geosciences and Civil Engineering' of the University of Karlsruhe in cooperation with the National Institute of Earth Physics (NIEP) in Bucharest. The network (Bonjer and Grecu, 2004) is operative since 1997 and consists of 44 digital Kinematics K2 instruments, mostly located in free-field conditions. The recordings from the 1986 earthquake as well as from the 1977 event (one recording only) are analogue observations from an SMA-1 network operated by NIEP (Oncescu et al., 1999a) which have been digitized.

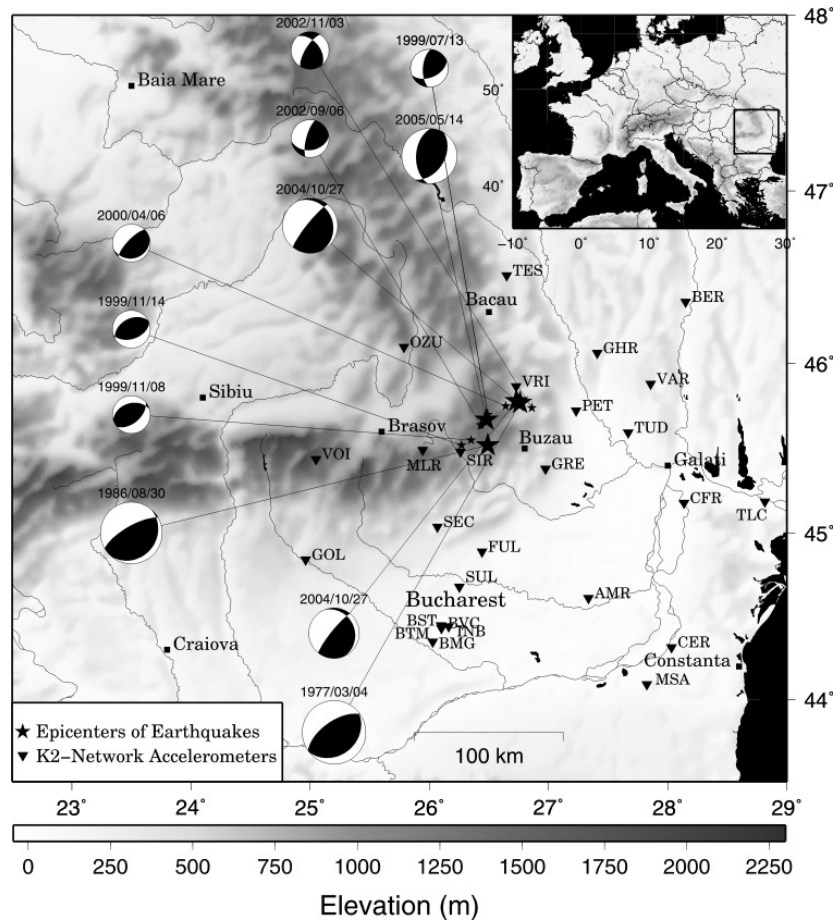


Figure 1: Topographic map of the Carpathian area. The Vrancea seismogenic zone is situated in the bend of the arc. The epicenters of the utilized earthquakes are marked by stars (big stars for the TARGET events) and the fault plane solutions of the events are also indicated (the corresponding EGF earthquakes are lined up in a column with the respective TARGET event). The K2 accelerometers which provided data for this study are depicted as inverse triangles.

In total, acceleration data from six EGF events ($4.0 \leq M_w \leq 5.0$) are used to model the 1986, 2004 and 2005 TARGET earthquakes. The 2004 event is itself used as EGF in order to simulate the 1977 TARGET earthquake. The hypocentral coordinates, origin times and depth information of the EGF earthquakes as well as of the TARGET events is listed in Table 1. The October 2004 earthquake is referred to as TARGET-1, the August 1986 event as TARGET-2, the 1977 one as TARGET-3 and, finally, the May 2005 earthquake as TARGET-4. The EGF earthquakes were chosen following the conditions that the focal mechanisms should be as similar as possible to the one of the TARGET and they should be located at approximately the same depth.

Fig. 1 shows the epicenters and the locations of the stations used in this study. Additionally, the focal mechanisms of all earthquakes are displayed. Each analyzed TARGET earthquake is marked by a large star, and the focal mechanisms of the EGF event(s) associated with it are lined up in a column with the TARGET's focal mechanism. The fault plane solutions of the main shocks are taken from the Harvard CMT catalogue, whereas those of the EGF earthquakes are from the ROMPLUS catalogue (Onescu et al., 1999b). The data recorded from the K2-network have been sampled with 200 samples/s, whereas the analogue SMA-1 recordings were digitized with a sampling rate of 100 samples/s. As a part of the digitization process, the SMA-1 records have been Ormsby filtered (for most stations between 0.125-24

Table 1: Hypocentral coordinates, moment magnitudes and origin times of the events used in this study. The smaller earthquakes used to generate the synthetics are marked by the identification code EGF whereas the respective large event is referenced to as TARGET. The information shown in this table was gathered from the ROMPLUS-catalogue (Oncescu et al., 1999a).

Event ID	Date	Origin Time	Lat [°]	Long [°]	Depth [km]	M _w
EGF1-200209	2002/09/06	05:04:02	45.64	26.43	105	4.1
EGF1-200211	2002/11/03	20:30:23	45.74	26.86	90	4.0
EGF2-19991108	1999/11/08	19:22:52	45.55	26.35	138	4.6
EGF2-19991114	1999/11/14	09:05:59	45.52	26.27	132	4.6
EGF2-200004	2000/04/06	00:10:39	45.75	26.64	143	5.0
EGF3-200410	2004/10/27	20:34:36	45.78	26.73	99	5.8
EGF4-199907	1999/07/13	13:10:58	45.70	26.49	132	4.0
TARGET-1	2004/10/27	20:34:36	45.78	26.73	99	5.8
TARGET-2	1986/08/30	21:28:37	45.52	26.49	132	7.1
TARGET-3	1977/03/04	19:21:54	45.77	26.76	94	7.4
TARGET-4	2005/05/14	01:53:21	45.68	26.54	140	5.2

Hz, but for some, as e.g. CFR, only between 0.125-15 Hz). Thus, in view of the frequency constraints imposed by the digitization process, any analysis performed with the SMA-1 data is restricted to frequencies lower than 12-15 Hz. In order to create a consistent database, the digital K2-recordings are downsampled to a sampling frequency of 100 Hz.

Only the horizontal components of the S-wave are used, as the strongest part of the shaking is usually found there. The data are rotated and, for the inversions, we finally used 15 s SH-wave signal windows that start 2 s before the S-wave onset, the latter one being picked on the velocity traces. A key point in using small earthquakes as EGFs to simulate larger ones is their signal-to-noise (SN) ratio, as only a frequency range with acceptable SN-ratio should be used in order to avoid scaling up noise instead of signal energy. The SN-ratio of the K2-data is, as a rule, larger than two up to frequencies between 20-25 Hz, although the most relevant part of the signal energy is associated with frequencies smaller than about 12 Hz. Records with unclear S-wave onset or unacceptable SN-ratio are removed from the dataset. Regarding the SMA-1 digitized data, no SN-ratio analysis is feasible, as these records do not include any relevant pre-event noise.

In total, 22 records (12 from EGF1-200209 and 10 from EGF1-200211) recorded at 14 locations were included in the inversion of TARGET-1, 14 records (5 from EGF2-19991108, 5 from EGF2-19991114 and 4 from EGF2-200004) recorded at 6 locations were used for TARGET-2 and 6 records from EGF4-199907 for the inversion of TARGET-4. Concerning the inversion of TARGET-3, acceleration data from the October 2004 event (TARGET-1 and EGF3-200410) at 33 locations was used. The considered frequency range (based on a signal-to-noise ratio analysis of EGF-C200410) was 0.2 – 12 Hz.

METHODOLOGY

Empirical Green's Functions Technique

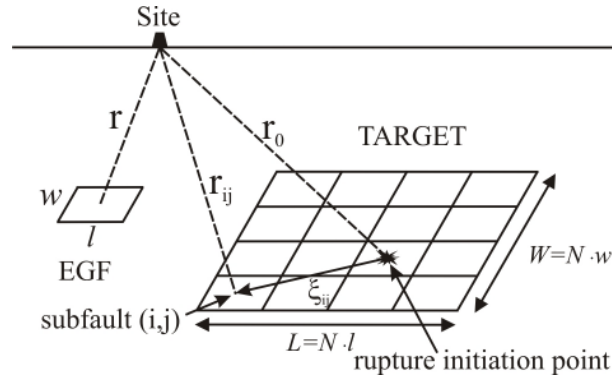


Figure 2: Illustration of the EGF technique of Irikura (modified after Oth et al., 2007).

Irikura's method is based on the self-similarity hypothesis, which in general assumes constant stress drop over a wide magnitude range. Detailed descriptions of the technique are given in Irikura (1983, 1986, 1999), Miyake et al. (2003) and Oth et al. (2007), and I refer the reader to these publications for a thorough discussion of the method. In brief, the fault plane of the large earthquake (TARGET) is constructed from N^2 subfaults of identical size (see Fig. 2), and N is determined by the following scaling laws (Irikura, 1999):

$$\frac{L}{l} = \frac{W}{w} = \frac{T_r}{t_r} = N \text{ and } \frac{\bar{D}}{d} = CN, \quad (3)$$

where l , w , \bar{d} and t_r denote the length, width, displacement and rise time of the EGF event and L , W , \bar{D} and T_r are the same parameters for the TARGET event. C is the stress drop ratio (dynamic and static) between the TARGET and EGF earthquake. In terms of seismic moments M_0 (TARGET) and m_0 (EGF), this means:

$$N = \sqrt[3]{\frac{M_0}{C m_0}}. \quad (4)$$

The source model on which the methodology is based is an extended area with homogeneous slip and rise time (e.g. Kamae and Irikura, 1998; Miyake et al., 2003). A physical interpretation for this source model has been given recently by Miyake et al. (2003), who, following the analysis of twelve crustal earthquakes in Japan, came to the conclusion that the SMGA is equivalent to an asperity within a larger rupture area, where the background slip area shows practically no stress release. The advantages of the method are that it neither requires the knowledge of the explicit shape of the slip velocity time function nor the direct estimation of path and site effects (as long as linear soil behavior is a valid approximation, which is considered to be reasonable in our case as the peak accelerations do not exceed 0.2 – 0.3 g, e.g. Su et al., 1998). On the other hand, it is not always easy to find an appropriate smaller event to be used as EGF, as it should have approximately the same location and focal mechanism and must be recorded at the same site as the target earthquake to be synthesized.

Estimation of Spectral Scaling Parameters C and N

For TARGET-1, -2 and -4, where enough waveform data are available, the scaling parameters C and N can be derived from the spectral ratios between the TARGET and EGF spectra (e.g. Miyake et al., 2003; Oth et al., 2007). In frequency domain, the seismic ground motion Fourier amplitude spectrum (FAS) can be described by:

$$U(f) = S(f) \cdot P(f) \cdot G(f), \quad (5)$$

where $U(f)$ is the observed spectrum, $S(f)$ the source, $P(f)$ the path and $G(f)$ the site contributions. For the TARGET and EGF earthquakes, the path and propagation effects are assumed to be the same, as mentioned earlier. If the source contributions show the ω^2 shape (Brune, 1970, 1971), the spectral ratio between TARGET ($U(f)$) and EGF ($u(f)$) is:

$$\frac{U(f)}{u(f)} = \frac{M_0}{m_0} \cdot \frac{1 + \frac{f^2}{f_{C,E}^2}}{1 + \frac{f^2}{f_{C,T}^2}}, \quad (6)$$

where $f_{C,T}$ and $f_{C,E}$ denote the respective corner frequencies. This ratio tends to a constant level both in the low and high frequency limits, which, as can be shown (see e.g. Oth et al., 2007), have the respective values CN^3 and CN . Thus, C and N can be derived from the spectral ratios. The results of this procedure are graphically displayed in Fig. 3 and listed in Table 2. For TARGET-3, the situation is complicated by the fact that there is only one strong motion observation available, which makes it impossible to provide a reasonable estimate of C and N from the spectral ratios. In view of the results obtained for the other TARGET earthquakes, C is set to 1 and $N=6$ is derived from Eq. (4). The result obtained in the inversion for this event can be cross-checked in several ways, which are discussed later.

Table 2: Parameters M_0/m_0 , $f_{C,T}$, $f_{C,E}$, N and C obtained from the spectral ratio analysis.

Event ID	$\frac{M_0}{m_0}$	$f_{C,T}$ [Hz]	$f_{C,E}$ [Hz]	N	C	Num. stat.
TARGET-1/EGF1-200209	211	1.7	8.3	5	1.7	12
TARGET-1/EGF1-200211	651	1.6	10.8	7	1.9	10
TARGET-2/EGF2-19991108	8144	0.3	4.0	16	2.0	5
TARGET-2/EGF2-19991114	7134	0.3	4.9	17	1.5	5
TARGET-2/EGF2-200004	914	0.3	3.1	11	0.7	4
TARGET-4/EGF4-199907	57	1.1	3.4	3	2.1	4

Inversion Procedure – The Genetic Algorithm

The SMGA is characterized by seven parameters: stress drop ratio C , scaling factor N , length L , width W , rise time T_r and rupture initiation point along strike and along dip. As C and N have already been determined, the number of free parameters is reduced to five (strictly speaking, the rupture and shear wave velocities would be additional parameters, which we regard as fixed, as otherwise the inversion results would be poorly constrained – different ratios of rupture to shear wave velocity were tested). Thus, the problem which shall be solved is a non-linear one depending on five controlling parameters. A good way to approach it is to evaluate many different trial models regarding a certain criterion and to exploit for instance the concept of the genetic algorithms (e.g. Goldberg, 1989) in order to find the minimum cost solutions for the SMGA source model of each TARGET earthquake.

Genetic algorithms work in three main steps:

- Natural selection (the fittest members of the population, i.e. those with lowest cost, survive, while those with highest cost die off)
- Mating and crossover (the survivors mate in pairs and produce offspring which carry the mixed traits of the parents)
- Mutation (random changes are included in the genetic information of the offspring)

The algorithm used is described in detail in Oth et al. (2007). For TARGET-1, -2 and -4, the cost function to be minimized is given by the L2-norm of the acceleration envelopes e and displacement waveforms u (frequency range 0.5 – 12 Hz for TARGET-1 and -4, 0.4 – 12 Hz for TARGET-2):

$$\text{cost} = \sum_{\text{records}} \left(\frac{\sum_t (u_{\text{obs}} - u_{\text{syn}})^2}{\sqrt{\sum_t u_{\text{obs}}^2 \sum_t u_{\text{syn}}^2}} + \frac{\sum_t (e_{\text{obs}} - e_{\text{syn}})^2}{\sqrt{\sum_t e_{\text{obs}}^2 \sum_t e_{\text{syn}}^2}} \right). \quad (7)$$

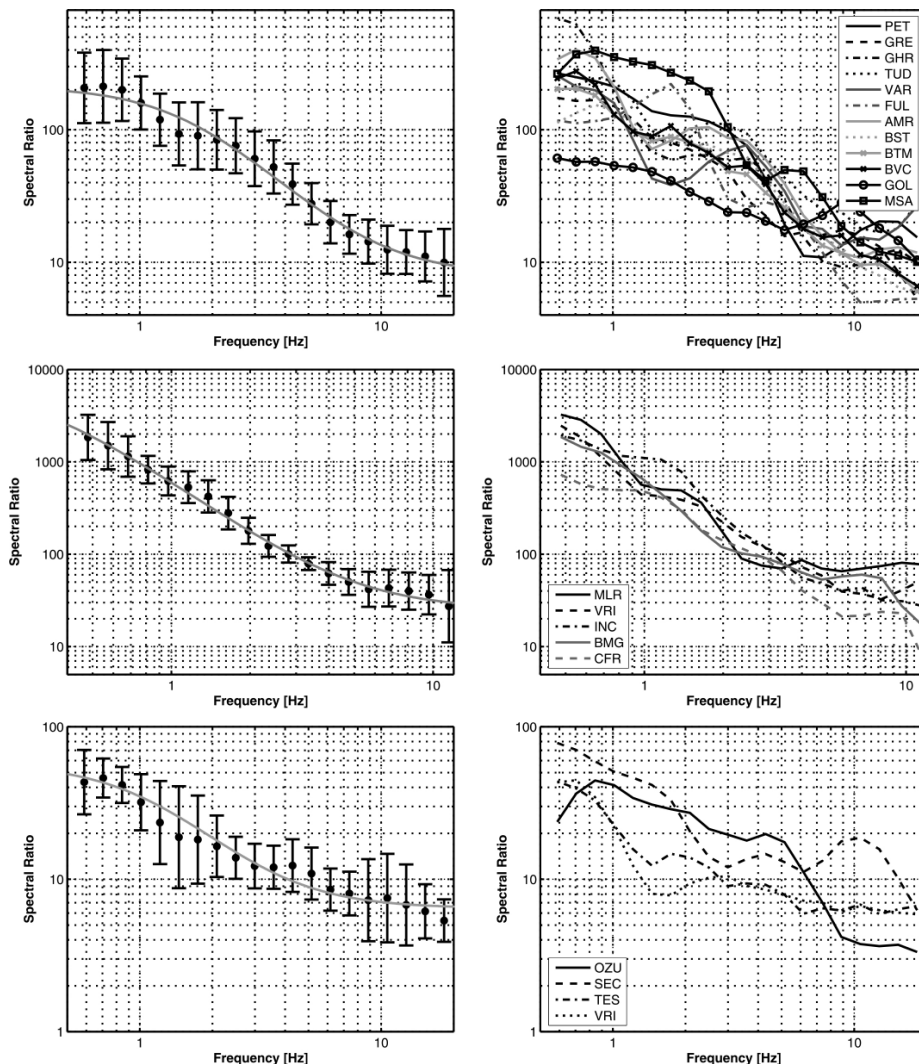


Figure 3: Spectral ratios in order to determine the scaling factors C and N . Top row: TARGET-1/EGF1-200209. Middle row: TARGET-2/EGF2-1999114. Bottom row: TARGET-4/EGF4-199907. The left column shows the logarithmic average with standard deviations and the theoretical curve fit, whereas the right column depicts the spectral ratios at the individual stations.

For TARGET-3, as already mentioned above, a waveform-based inversion is not possible. Therefore, we used the technique of Sokolov (2002) to determine instrumental intensities from each set of simulations (at 33 locations, using EGF3-200410 respectively TARGET-1 as EGF earthquake) and compared these simulated intensities with the observed macroseismic intensity map (Radu et al., 1979) using the L1-norm:

$$\text{cost} = \sum_{\text{records}} (|Intensity_{\text{observed}} - Intensity_{\text{simulated}}|). \quad (8)$$

The frequency range utilized in this inversion was 0.2 – 12 Hz. The observed recording at station Incerc in the city of Bucharest as well as the results of the inversion for TARGET-1 are used as additional information to check the plausibility of the obtained results for TARGET-3. First, the subelement size for TARGET-3 should be approximately identical to the SMGA size of TARGET-1. Second, the intensity derived SMGA source model should, if it is correct, also be able to explain the first-order characteristics of the observed recording of TARGET-3. As we show below, both these requirements are indeed fulfilled. As the inversion is not based on waveform data and the intensity computation after Sokolov (2002) relies on the FAS (thus, no phase information is included in the inversion), we enforced one further constraint: the aspect ratio of the SMGA was fixed, once to be a square, once to have an aspect ratio $L:W=1:1.5$.

RESULTS AND DISCUSSION

The search ranges for the parameters were set to 0.5 – 15 km for L and W and 0.01 – 2 s for T_r during the inversion for the source parameters for TARGET-1 ($M_W = 5.8$) and TARGET-4 ($M_W = 5.2$), 1 – 40 km for L and W and 0.05 – 5 s for T_r during the inversion of TARGET-2 ($M_W = 7.1$) and 2.5 – 60 km for L (W was computed from the enforced aspect ratio) and 0.05 – 5 s for T_r during the inversion of TARGET-3 ($M_W = 7.4$). All subfaults were searched for the rupture starting point location. For TARGET-1 and -2, we performed a combined inversion with all respective EGF-events. The inversion results with lowest cost values are summarized in Table 3. For TARGET-1 and -4, the lowest cost was found for a ratio of rupture to shear wave velocity of $v_R/v_S=0.9$, whereas for TARGET-2, the lowest cost was found for $v_R/v_S=0.7$ (we tested $v_R/v_S=0.7, 0.8$ and 0.9 , with $v_S=4.5$ km/s). For TARGET-3, the inversion was run with $v_R/v_S=0.9$ only in view of the results for TARGET-1 and the fact that the intensity-based inversion is computationally more time consuming. The genetic algorithm was run 5 times for each v_R/v_S to check the stability and uniqueness of the solution.

Table 3: Lowest cost SMGA models resulting from 5 consecutive runs of the genetic algorithm for each target event with $v_R/v_S=0.7, v_R/v_S=0.8, v_R/v_S=0.9$ for TARGET-1, -2 and -4. For TARGET-3, the algorithm was run 5 times with $v_R/v_S=0.9$ in view of the results obtained for TARGET-1. The position of rupture initiation is given as normalized value in the interval [0 1] for TARGET-1 and -2, as these events have been inverted using several EGFs, whereas it is given absolutely for TARGET-3 and -4.

TARGET	v_R/v_S	L [km]	W [km]	T_r [s]	pos. along strike	pos. along dip
1	0.9	1.16	1.78	0.11	0.3	0.7
2	0.7	12.84	12.60	0.26	0.4	1.0
3 (square)	0.9	8.13	8.13	0.96	1	4
4	0.9	3.04	3.67	0.08	1	3

Waveforms and Intensity Pattern

Several waveform examples in order to illustrate the fit between simulated (with the lowest cost models given in Table 3) and observed time histories are shown in Fig. 4 (TARGET-1). In general, the fit ranges from fair to very good, even though in some cases the peak amplitudes are slightly misestimated (with a maximum factor of about 2). The outcome of the macroseismic intensity inversion for TARGET-3 is shown in Fig. 5, where the observed isoseismals are depicted as black lines. Although the scatter is rather large, the main features can be reproduced acceptably well. If only the simulated intensities were known, one would probably draw a continuous isoseismal line of value VIII around the epicentral area and Bucharest instead of separate patches. Only the small patch of intensity VIII around Craiova cannot be reproduced with our data.

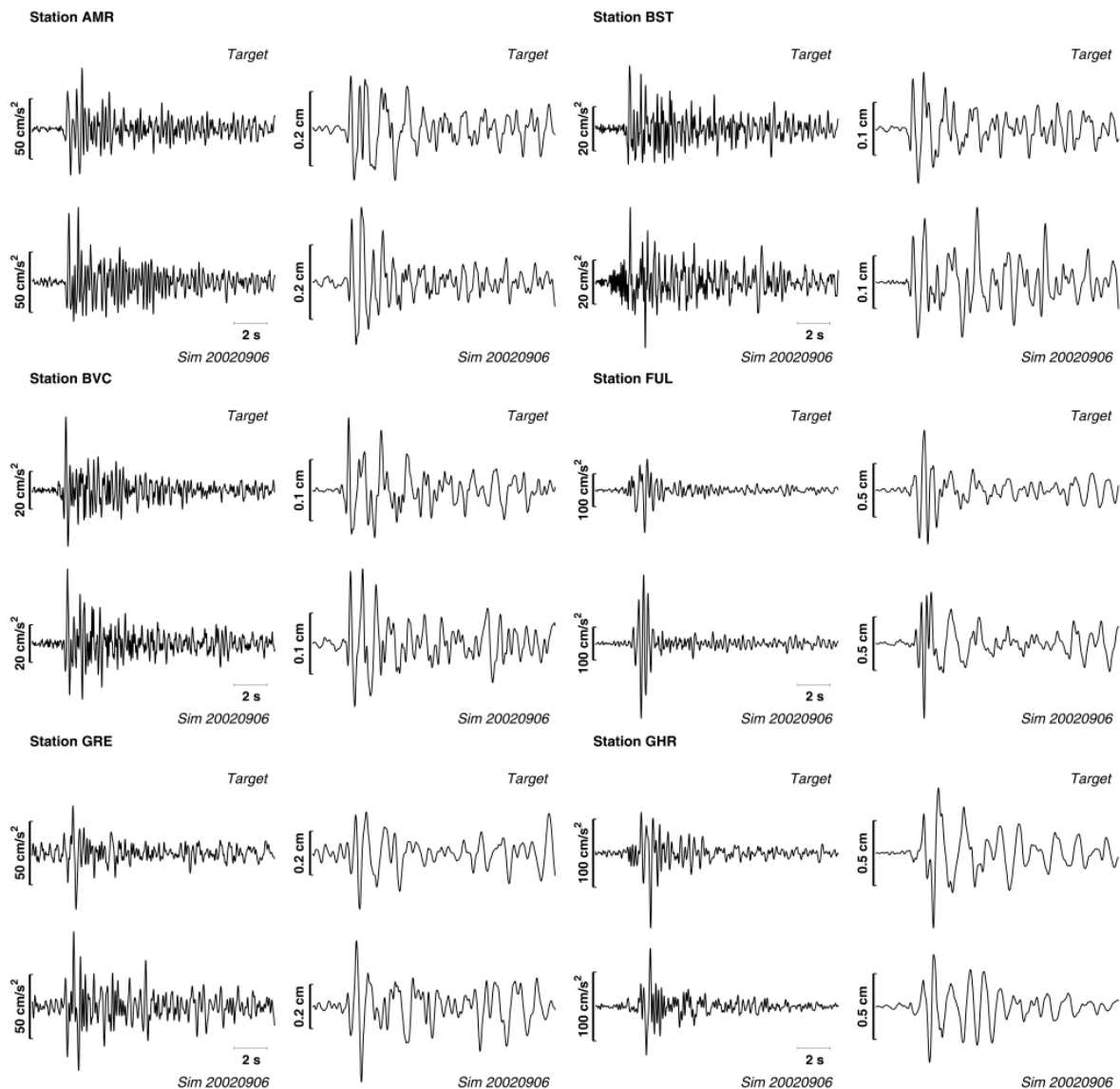


Figure 4: Waveform examples simulated for TARGET-1 (using EGF-200209) with the lowest cost SMGA source model. For each station, the observed (top) and simulated (bottom) acceleration (left) and displacement (right) 15 s SH-waveforms are displayed. Each set of corresponding observations and simulations is scaled to the same maximum value.

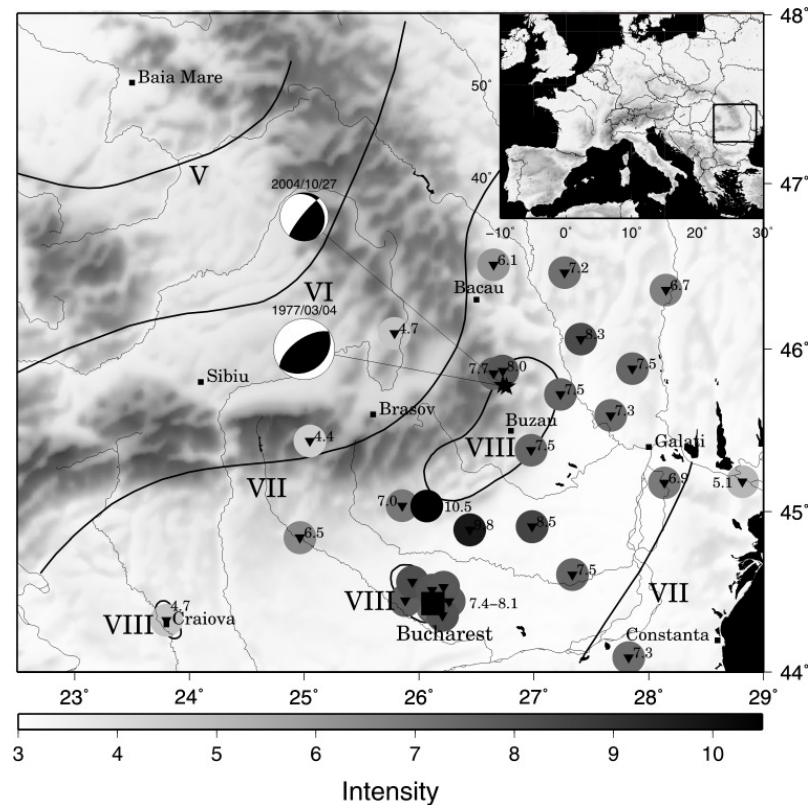


Figure 5: Comparison of simulated and observed intensities (MSK) for TARGET-3. The isoseismals of the observed intensity pattern are shown as black lines. The value of the simulated intensity is written close to each station. The epicenters and focal mechanisms of TARGET-3 and EGF-200410 (resp. TARGET-1) are additionally displayed.

Uniqueness of the Solutions

For TARGET-1, -3 and -4, the solutions from several runs of the algorithm were very similar and thus, for these events, the inverted solutions can be regarded to be well constrained. This is not the case for TARGET-2 with $v_R/v_S=0.9$, as can be seen from the histogram plots for the 750 best solutions found in 5 runs shown in Fig. 6. On the left side, the histograms for $v_R/v_S=0.8$ are shown, whereas on the right hand side, the ones for $v_R/v_S=0.9$ are depicted.

Clearly, for $v_R/v_S=0.9$, the width W and rupture initiation point along dip present at least three possible values, whereas the rise time shows a second peak around 1.3 s. Interestingly, the rupture length and rupture starting point along strike are well constrained. On average, the costs of the best models for $v_R/v_S=0.9$ are about 10-15 % higher than the cost of the best ones for $v_R/v_S=0.8$, which leads to the conclusion that the former models are less probable. Yet, the differences in cost are not large enough to strictly rule them out, and this ambiguity for TARGET-2 has to be kept in mind during the oncoming discussion.

Physical Interpretation and Discussion

The lowest cost SMGA source models for the four earthquakes treated in this article are depicted schematically in Fig. 7. The SMGA dimensions and rise times obtained during the inversion for TARGET-1 and -3 are remarkably small (around 2 km² for TARGET-1, 65-90 km² for TARGET-3). For TARGET-2 and -4, they are somewhat larger (approximately 160 km² for TARGET-2 and 12 km² for TARGET-4). The rise times are very small for all four

analyzed Vrancea earthquakes, which directly leads to the conclusion that all of these events show a high particle velocity.

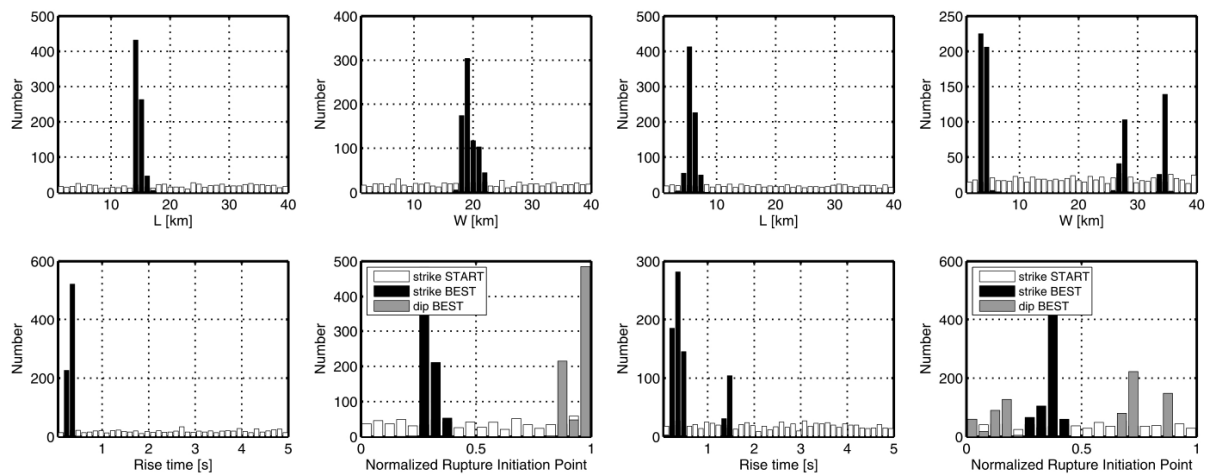


Figure 6: Histograms of the 750 best solutions found during 5 runs of the genetic algorithm for the SMGA parameters of TARGET-2. Left: Histograms for $v_R/v_S=0.8$. Right: Histograms for $v_R/v_S=0.9$. The white bars indicate the distribution of the starting models in the initial generation of the 5 runs.

Regarding TARGET-3, it is encouraging to see that the lowest cost SMGA model can explain the observed record at station Incerc (named INB in this study) quite well (see Fig. 8). Moreover, the SMGA size for TARGET-1 is in good agreement with the subfault size of TARGET-3. First, this is a good indication that it was not a completely false estimate to use the stress drop ratio $C = 1$ between these two events. Secondly, it should be emphasized at this point that the waveform inversion for the SMGA parameters of TARGET-1 and the intensity pattern inversion performed for TARGET-3 both provide information on TARGET-1's SMGA which is essentially independent of each other and leads to very similar SMGA sizes and rise times for the October 2004 earthquake (once as the main shock, once as the subevent). Thus, these results are indeed consistent with each other. Radulian et al. (2007) determined similar dimensions for this event's asperity from the pulse width of the source time function after deconvolution of an empirical Green's function.

Miyake et al. (2003) interpreted the SMGA to be equivalent to an asperity in the stress-free field based on a dataset of crustal earthquakes where low-frequency slip inversions were available. Such slip inversions do unfortunately not exist for the intermediate-depth Vrancea earthquakes. In order to estimate the spatial extent of the total rupture plane, the only source of information that we can rely on is the aftershock distribution. The dimensions of the total rupture area are needed in order to estimate which part of the seismic moment is released by the SMGA compared to the background slip area. For TARGET-2 (1986), Oncescu (1989) proposed an asperity of about 160 km^2 within a total rupture area of about 700 km^2 , the latter one having been estimated by the occurrence of aftershocks. The size of our lowest cost SMGA is surprisingly close to this asperity size estimate. For TARGET-1 (2004), the situation is complicated by the fact that very few aftershocks occurred (Bonjer, pers. comm., 2006), which makes it impossible to estimate the extent of the rupture using this information. For TARGET-3 (1977), Hartzell (1979) and Räckers and Müller (1982) proposed fault plane dimensions ranging around 2000 km^2 .

If we follow the interpretation of Miyake et al. (2003), the SMGA is considered to be an asperity within a larger background slip area which is assumed to have no stress drop. Based on the work of Madariaga (1979) and Boatwright (1988), they proposed to estimate the stress drop of the SMGA with the following equation, assuming a single asperity model:

$$\Delta\sigma_{SMGA} = \frac{7}{16} \cdot \frac{M_0}{Rr^2}, \quad (9)$$

where M_0 is seismic moment of the earthquake, R is the radius of the equivalent circular total rupture plane and r is the radius of the equivalent circular SMGA. Formula (9) means nothing else than computing the stress drop for a circular crack of radius r with a seismic moment reduced by the factor r/R to account for the moment release due to the background slip. We can then (with this reduced seismic moment) use the definition $M_0 = \mu \cdot A \cdot \bar{D}$, with A being the fault (or asperity) area and \bar{D} its average displacement, and the rise time T_r to compute estimates for the slip and slip velocity within the SMGA.

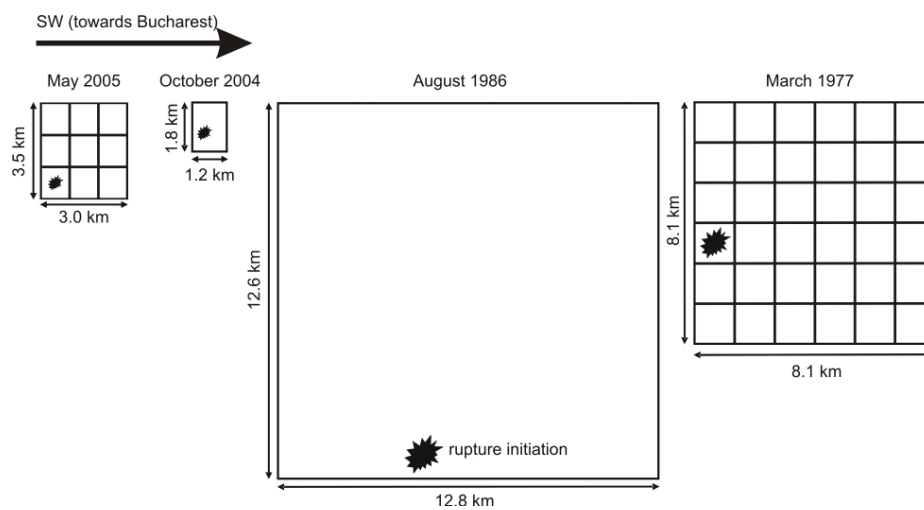


Figure 7: Sketches of the lowest cost SMGA models for the four Vrancea earthquakes analyzed. The relative dimensions are scaled correctly and the rupture initiation location is depicted by a star. Note the very similar size of the subfault of the March 1977 (TARGET-3) and the SMGA of the October 2004 (TARGET-1) events.

With the SMGA- and total rupture area estimates discussed above, the approximate values listed in Table 4 have been computed (assuming $\mu = 7 \cdot 10^{10} \text{ N/m}^2$). The stress drop for the October 2004 event has been deduced from the one of the March 1977 event (remember that we set their stress drops to be equal). From this stress drop estimate and the SMGA size, a total fault plane area of approximately $30 - 40 \text{ km}^2$ can be deduced for the October 2004 earthquake.

Two major interesting conclusions arise from these results. First, the March 1977 as well as the October 2004 earthquakes seem to show 2 – 3 times larger (static) stress drops than the August 1986 event. The second striking feature is the fact that all the events analyzed seem to be similar from the dynamic point of view, as they depict almost identical particle velocities and thus (see Eq. (1)), almost identical dynamic stress drops ranging around 1kbar. These large particle velocities are responsible for the strong high-frequency radiation. These stress drops and particle velocities are about one order of magnitude larger than for crustal earthquakes. Miyake et al. (2003) showed that the SMGA is equivalent to an asperity of about 100 bar stress release for crustal earthquakes.

These large stress drops and particle velocities should also be taken into consideration when assessing seismic hazard, as they imply a higher energy release than for typical crustal earthquakes.

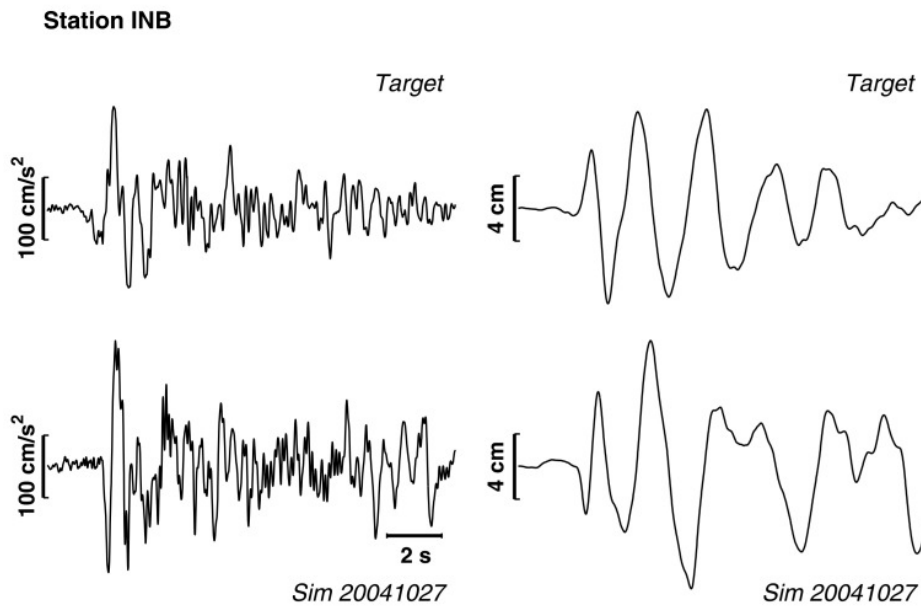


Figure 8: Comparison of acceleration (left) and displacement (right) observed (top) and simulated (bottom) EW component waveforms at station Incerc (named INB) of TARGET-3.

A final interesting issue is the strong damage produced in Bucharest city during the 1977 earthquake, whereas the city was not that heavily harmed during the 1986 event. As can be seen from Fig. 7, the directivity effect towards Bucharest within the SMGA is larger for the 1977 earthquake than for 1986, but it may be questioned whether this effect alone and the somewhat higher magnitude in 1977 is enough to explain the quite large differences in macroseismic intensities. As the 1977 earthquake apparently showed a larger stress release, this might also be a decisive component contributing to the differences in intensity level. As the SMGA size for the October 2004 earthquake is exceptionally small, directivity effects are probably less relevant for this event.

Table 4: Approximate stress drop, particle velocity and slip estimates for the lowest cost SMGA models for TARGET-1, -2 and -3. For TARGET-4, there is no information on background fault dimensions, which makes it impossible to provide an estimate for these parameters.

Event ID	$\Delta\sigma_{SMGA}$ [bar]	$\langle\dot{U}\rangle$ [m/s]	\bar{D} [m]
TARGET-1 (October 2004)	900 – 1200	3.5 – 4.5	0.8 – 1.0
TARGET-2 (August 1986)	300	4.0	2.2
TARGET-3 (March 1977)	900	3.5	5.0
	1200	3.0	5.5

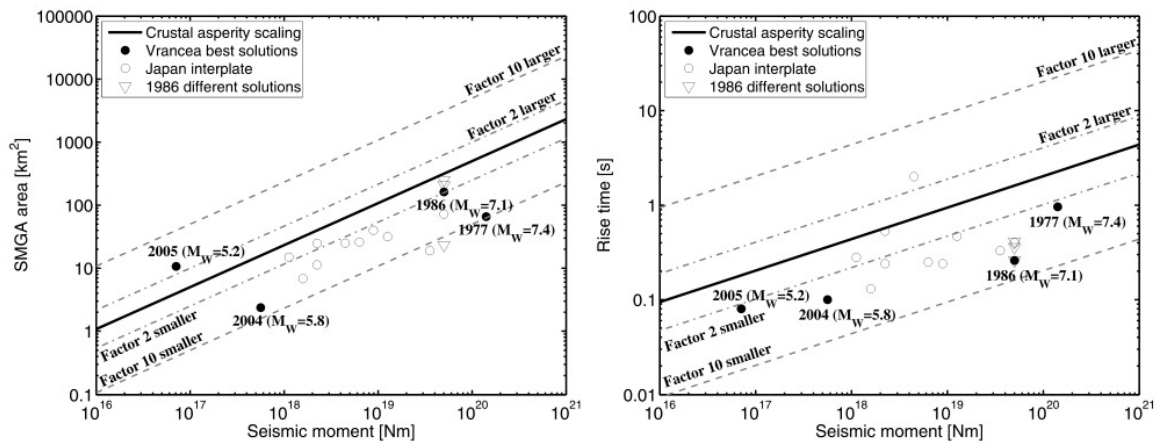


Figure 9: Left: Scaling of the SMGA size with seismic moment. Right: Scaling of the rise time with seismic moment. The black line represents the scaling for crustal asperities as given by Somerville et al. (1999) (the grey dotted lines indicate sizes a factor of 2 and 10 smaller/larger than this scaling). The black dots depict the best solutions for the four Vrancea earthquakes treated in this work. As the results for the 1986 (TARGET-2) earthquake are ambiguous, the different 'best' solutions with similar cost are plotted with open triangles. The results for Japanese interplate earthquakes (Suzuki and Iwata, 2005) are shown by open circles.

The scaling behavior of the SMGA size and rise time with seismic moment is graphically displayed in Fig. 9. The black line in these figures represents the scaling relations empirically determined by Somerville et al. (1999) for crustal earthquakes from low frequency finite-fault rupture models. As can be seen, the SMGA dimensions are smaller by a factor up to 10 for the four Vrancea earthquakes treated in this study. Only the 2005 earthquake (TARGET-4) shows an SMGA size a bit larger than expected for a crustal SMGA (Miyake et al., 2003, show that the SMGA of crustal earthquakes closely follows the scaling of Somerville et al., 1999). The rise time is systematically smaller than the one expected for crustal earthquakes by a factor of 2-8, which indicates that the particle velocity will also be larger. Miyake et al. (2003) conclude that the crustal SMGA, which obeys Somerville et al.'s (1999) scaling relations, corresponds to a 100 bar (static) stress drop asperity. Thus, if, on average, the SMGA size of Vrancea earthquakes is smaller by a factor of about 5, the static stress drop will be, on average, larger by roughly an order of magnitude. Consequently, even though four earthquakes are of course not a very large dataset (nevertheless, it is the largest dataset of moderate to strong Vrancea earthquakes in terms of high-quality recordings ever analyzed), the results presented here lead to the conclusion that the intermediate-depth Vrancea earthquakes are inherently different from crustal ones.

Do intermediate-depth earthquakes in other areas of the world show similar source characteristics? Suzuki and Iwata (2005) present SMGA parameters from a very similar study than the one performed in this work for ten Japanese interplate earthquakes (with depths ranging between 30 and 50 km, which is shallower than the Vrancea events, but yet larger than for typical crustal earthquakes), which are included as a means of comparison in Fig. 9. These earthquakes seem to show a very similar scaling behavior of the SMGA, although the scatter (especially in the rise time estimates) is also rather large. Within the uncertainty ranges, the results obtained for the four Vrancea earthquakes can be regarded to be compatible with the ones of Suzuki and Iwata (2005). Thus, there is a line of evidence which leads to the conclusion that the scaling of the SMGA's (respectively asperities) for intermediate-depth and subcrustal interplate earthquakes seems to be different of the one for crustal earthquakes. The former ones show a larger particle velocity and static stress drop, and these facts have to be taken into account when performing strong motion simulations and when assessing seismic hazard from this type of earthquakes.

CONCLUSIONS

The empirical Green's functions method of Irikura was used to gain more insights into the source processes of intermediate-depth Vrancea earthquakes. In this study, the largest number of high quality strong motion data ever available for a source study of Vrancea earthquakes has been used to determine source models for the moderate size October 27th 2004 ($M_W = 5.8$) and May 14th 2005 ($M_W = 5.2$) and the two large March 4th 1977 ($M_W = 7.4$) and August 30th 1986 ($M_W = 7.1$) events. The application of Irikura's method to Vrancea earthquakes leads to small strong motion generation areas. According to the definition of Miyake et al. (2003), these areas (inside of which constant slip and slip velocity is supposed) are interpreted as asperities within a total background fault plane with practically no stress drop. Therefore, for a given seismic moment, a smaller strong motion generation area and rise time is equivalent to higher stress drops and particle velocities. Our results show stress drop and particle velocity values within these asperities ranging between 300 and 1200 bar and 3 and 5 m/s respectively. Crustal earthquakes usually show stress drop values between 10 and 100 bar and particle velocities lower than 1 – 2 m/s (e.g. Kanamori, 1994). Miyake et al. (2003) presented evidence that the strong motion generation areas of crustal earthquakes show a stress release of about 100 bar. Thus, the events treated here are inherently different. The large particle velocities imply a particularly efficient high-frequency radiation. These facts are of high importance for strong ground motion prediction for large earthquakes in the area and have to be taken into account when assessing Romania's seismic hazard.

ACKNOWLEDGMENTS

This study was carried out in the Collaborative Research Center (CRC) 461 'Strong Earthquakes: a Challenge for Geosciences and Civil Engineering', which is funded by the Deutsche Forschungsgemeinschaft (German Research Foundation) and supported by the state of Baden-Württemberg and the University of Karlsruhe. We thank K. Irikura and H. Miyake for providing their simulation program and their advice on its use. V. Sokolov kindly made his instrumental intensity code available to us.

REFERENCES

- Bonjer, K-P. and B. Greu (2004). Data release 1996 – 2004 of the Vrancea K2 seismic network. One DVD with evt files, Bucharest-Karlsruhe.
- Boatwright, J. (1988). The seismic radiation from composite models of faulting. *Bull. Seism. Soc. Am.*, 78, 489-508.
- Brune, J.N. (1970). Tectonic stress and the spectra of seismic shear waves from earthquakes. *J. Geophys. Res.*, 75, 4997-5009.
- Brune, J.N. (1971). Correction. *J. Geophys. Res.*, 76, 5002.
- Goldberg, D.E. (1989). Genetic Algorithms in Search, Optimization and Machine Learning. Addison-Wesley, New York.
- Hartzell, S. (1979). Analysis of the Bucharest strong ground motion record for the March 4, 1977 Romanian earthquake. *Bull. Seism. Soc. Am.*, 69, 513-530.
- Irikura, K. (1983). Semi-Empirical Estimation of Strong Ground Motions during Large Earthquakes. *Bull. Dis. Prev. Res. Inst., Kyoto Univ.*, 33, Part 2, No. 298, 63-104.
- Irikura, K. (1986). Prediction of strong acceleration motions using empirical Green's function, in *Proceedings of the 7th Japan earthquake engineering symposium*, 151-156.
- Irikura, K. (1999). Techniques for the simulation of strong ground motion and deterministic seismic hazard analysis, in *Proceedings of the advanced study course seismotectonic and microzonation techniques in earthquake engineering: integrated training in earthquake risk reduction practices*, Kefallinia, 453-554.

- Kamae, K. and K. Irikura (1998). Source Model of the 1995 Hyogo-ken Nanbu Earthquake and Simulation of Near-Source Ground Motion. *Bull. Seismol. Soc. Am.*, 88, 400-412.
- Kanamori, H. (1994). Mechanics of earthquakes. *Ann. Rev. Earth Planet. Sci.*, 22, 207-237.
- Kanamori, H. and D. L. Anderson (1975). Theoretical basis of some empirical relations in seismology. *Bull. Seism. Soc. Am.*, 65, 1073-1095.
- Madariaga, R. (1979). On the relation between seismic moment and stress drop in the presence of stress and strength heterogeneity. *J. Geophys. Res.*, 84, 2243-2250.
- Martin, M., F. Wenzel and the CALIXTO working group (2006). High-resolution teleseismic body wave tomography beneath SE-Romania (II): Imaging of a slab detachment scenario, *Geophys. J. Int.*, 164, 579-595.
- Miyake, H., T. Iwata and K. Irikura (2003). Source characterization for broadband ground-motion simulation: Kinematic heterogeneous source model and strong motion generation area. *Bull. Seism. Soc. Am.*, 93, 2531-2545.
- Oncescu, M. C. (1989). Investigation of a high stress drop earthquake on August 30, 1986 in the Vrancea region. *Tectonophysics*, 163, 35-43.
- Oncescu, M. C. and K.-P. Bonjer (1997). A note on the depth recurrence and strain release of large Vrancea earthquakes. *Tectonophysics*, 272, 291-302.
- Oncescu, M. C., V. I. Marza, M. Rizescu and M. Popa (1999a). The Romanian earthquake catalogue between 984-1997, in *Vrancea earthquakes: tectonics, hazard and risk mitigation*, F. Wenzel, D. Lungu and O. Novak, Editors, Kluwer Academic Publishers, Dordrecht, Netherlands, 43-48.
- Oncescu, M. C., K.-P. Bonjer and M. Rizescu (1999b). Weak and strong ground motion of intermediate depth earthquakes from the Vrancea region, in *Vrancea earthquakes: tectonics, hazard and risk mitigation*, F. Wenzel, D. Lungu and O. Novak, Editors, Kluwer Academic Publishers, Dordrecht, Netherlands, 27-42.
- Oth, A., F. Wenzel and M. Radulian (2007). Source parameters from intermediate-depth Vrancea (Romania) earthquakes from empirical Green's functions modeling. *Tectonophysics*, 438, 33-56.
- Plenefisch, T. (1996). Untersuchungen des Spannungsfeldes im Bereich des Rheingrabens mittels der Inversion von Herdflächenlösungen und Abschätzung der bruchspezifischen Reibungsparameter. *Ph. D. Dissertation*, Universität Karlsruhe (TH), Germany, 128 pp.
- Radu, C., G. Polonic and I. Apopei (1979). Macroseismic field of the March 4, 1977 Vrancea earthquake. *Tectonophysics*, 53, 185-186.
- Radulian, M., K-P Bonjer, E. Popescu, M. Popa, C. Ionescu and B. Grecu (2007). The October 27th, 2004 Vrancea (Romania) earthquake. *ORFEUS newsletter*, 7, no. 1.
- Räkers, E. and G. Müller (1982). The Romanian earthquake of March 4, 1977: III. Improved focal model and moment determination. *J. Geophys.*, 50, 143-150.
- Sokolov, V. Yu. (2002). Seismic intensity and Fourier acceleration spectra: Revised relationships. *Earthquake Spectra*, 18, 161-187.
- Sperner, B., F. P. Lorenz, K.-P. Bonjer, S. Hettel, B. Müller and F. Wenzel (2001). Slab break-off - abrupt cut or gradual detachment? New insights from the Vrancea region (SE Carpathians, Romania). *Terra Nova*, 13, 172-179.
- Su, F., J. G. Anderson and Y. Zeng (1998). Study of weak and strong ground motion including nonlinearity from the Northridge, California, earthquake sequence. *Bull. Seism. Soc. Am.*, 88, 1411-1425.
- Suzuki, W. and T. Iwata (2005). Source characteristics of interplate earthquakes in northeast Japan inferred from the analysis of broadband strong-motion records. *Eos Trans. AGU*, 86 (52), Fall Meet. Suppl., Abstract S43A-1040.